ISSN 0016-7029, Geochemistry International, 2006, Vol. 44, No. 12, pp. 1170–1180. © Pleiades Publishing, Inc., 2006.
Original Russian Text © O.V. Vasyukova, V. I. Fonarev, 2006, published in Geokhimiya, 2006, No. 12, pp. 1266–1278.

Experimental Modeling of the Transformation of H_2O–CO_2–CH_4 Inclusions during Isobaric Cooling and Isothermal Compression

O. V. Vasyukova and V. I. Fonarev

Institute of Experimental Mineralogy, Russian Academy of Sciences, Chernogolovka, Moscow oblast, 142432 Russia
E-mail: mruk@iem.ac.ru, fonarev@iem.ac.ru

Received March 3, 2005

Abstract—The transformations (density, composition, or shape alterations) of fluid inclusions under isobaric cooling and isothermal compression have been experimentally modeled. The H_2O–CO_2–CH_4 inclusions used in the model experiments have been synthesized in quartz at 1 or 3 kbar and 700°C. The parameters of the model experiments were as follows: for isobaric cooling, 700–400°C at 1 or 3 kbar; for isothermal compression, 1–3 and 3–5 kbar at 400 and 700°C, respectively. The shape of the inclusion walls changed as a result of the experiments because of the dissolution and reprecipitation of the host phase. The intensity of these changes was directly affected by the pressure and temperature differences and the amount of the aqueous phase in the inclusions. Fluid densities increased in many inclusions in the run products: the increase ranged from insignificant (0.06 g/cm^3) to fairly noticeable (0.15 g/cm^3). The composition of the fluid inclusions also changed. The results of the experiments, in particular of those carried out with a *labeled* fluid, show that the penetration of a denser external fluid into inclusions with a lower fluid density is the basic reason for the increase in the density and change in the composition of fluid inclusions. In several experiments, the methane concentration changed with an attendant change in the melting temperature of carbon dioxide but without noticeable changes in the carbon dioxide homogenization temperature.

DOI: 10.1134/S0016702906120020

Fluid inclusions in minerals entrapped during mineral crystallization and subsequent rock transformations are the only direct source of information about the composition and density of the fluid in plutonic processes. Data interpretation encounters serious difficulties, especially for metamorphic rocks, because of a substantial postentrapment evolution of these inclusions. In many cases, both the density and the composition of inclusions change. The density can decrease (see [1] and other sources) because of the loss of some fluid (e.g., water is lost from H_2O–CO_2 inclusions), or it can even increase upon subisobaric cooling of rocks [2, 3]. The composition of inclusions can change as a result of a selective leakage of some amount of the primary fluid; not only water is removed (which is fairly usual for metamorphic processes), but nitrogen or methane is removed also [4]. The above facts necessitated experimental investigations in order to elucidate the scenarios and scales of the postentrapment evolution of the composition and density of fluid inclusions and the possibility of employing them for interpreting geological processes. The following essential issues remain unclear: the reasons and scenarios for the formation of high-density inclusions, whose density increases during the retrograde metamorphic evolution of rocks rather than decreases, as in most cases. In natural settings such inclusions were found in various regions [5, 6]; they were very informative for the interpretation of metamorphism. As a rule, the increase in the inclusion density is related to the decrease in the inclusion volume under isobaric cooling or isothermal compression. There are numerous experimental simulations of the evolution of aqueous inclusions in these conditions [7–10]. Bakker and Jansen [11–13] studied the behavior of H_2O–CO_2 inclusions. They and also Kotel'nikova and Sonyushkin [14] comprehensively considered the effect of dislocations on the migration of fluid components in quartz and the role of diffusion in this migration. Kalyuzhnyi [15] studied the properties of methane-containing inclusions during isothermal compression. These studies confirmed the data that the density and bulk composition of fluid inclusions can undergo substantial transformation in response to changing P–T parameters. However, the conclusions about the reasons and scenarios of this transformation are frequently at variance. Sterner and Bodnar [7] and Vityk and Bodnar [8] focus on the morphology of inclusions and arrive at the conclusion that the shape of inclusions is altered appreciably during isobaric cooling and isothermal compression, and these alterations do not resemble those induced by isobaric heating and isothermal decompression, respectively. Kalyuzhnyi's data [15] show that the inclusion shape remained unaltered during isothermal compression. The isobaric cooling and isothermal compression experiments carried out by Sterner and Bodnar [7] and Vityk and Bodnar [8] unam-

biguously demonstrated an increase in the fluid density, which the authors believe was due to the decrease in the inclusion volume. Bakker and Jansen [11–13] observed in their experiments that the density of H_2O–CO_2 inclusions decreased in the same conditions.

The above-cited experimental investigations, on the whole, showed that, in principle, the density of primary inclusions can noticeably increase during retrograde metamorphism. Unfortunately, there is no full understanding of this process. Does the density of the primary fluid in inclusions increase together with the deformation (the reduction in size) of vacuoles (e.g., during isobaric cooling or subisothermal compression)? Or could the penetration of the external, denser fluid (under the same conditions of isobaric cooling or subisothermal compression) be the main reason? Are there other scenarios that can generate superdense inclusions in metamorphic rocks? Does isobaric cooling or isothermal compression always cause an increase in fluid inclusion density?

If answers to these questions were found, the interpretation of microthermometric and cryometric data would be more substantiated and we would be able to more adequately judge the characteristic signs of the increasing density (whether the vacuole volume decreases or, by contrast, increases with the development of microfracture and dislocation systems), the deformation type (plastic or brittle) as a result of which such inclusions are expected to form, the composition of fluid inclusions (e.g., whether they correspond to the primary fluid or contain some new components), their densities (e.g., whether the observed inclusion density reflects real tectonothermal processes), and some other points.

One major goal of this work was to explore the reasons for the increased density of fluid inclusions. In choosing H_2O–CO_2–CH_4 inclusions to use in our experiments, we were guided by the abundance of such inclusions in metamorphic assemblages.

EXPERIMENTAL

The experiments were carried out on UVD 10000 hydrothermal equipment with an external heater designed at the Institute of Experimental Mineralogy, which is a modification of a known apparatus [16]. Two-section furnaces created a gradient-free zone of at least 5 cm in reactors in which an ampoule with the test sample was placed. Temperature monitoring was performed with a Chromel–Alumel thermocouple, which was mounted at the outer wall of the reactor within the gradient-free zone. The temperature was monitored automatically; the daily temperature drift was no greater than 5°C. The time to put the equipment into operation was about 1.5 h; the quenching time in flowing air to 150–200°C was 10–15 min. The pressure was measured with a pressure gauge with an error of ±50–100 bar. The experiments were carried out in platinum ampoules; a Ni–NiO buffer was used for the external control of oxygen fugacity. The ampoule sealing was verified by reweighing the ampoule after the experiment was over. The general scheme of the experiment was as follows: sample preparation (etching of quartz rods with hydrofluoric acid to generate pits on their surface) ⟶ synthesis of fluid inclusions of a given composition ⟶ investigation of the inclusions ⟶ modeling of isobaric cooling or isothermal compression using the samples synthesized ⟶ reinvestigation of the inclusions.

The quartz rods used in the experiments, either synthetic or natural, were $1 \times 1–2 \times 10$ mm in size and cut normal to axis *c*. A test sample was etched with hydrofluoric acid until noticeable surface pits were formed; after being carefully washed and dried, the sample was transferred to an ampoule that contained amorphous silica and a fluid, which was either oxalic acid or silver oxalate mixed with water. The inclusions were synthesized at $T = 700$°C and $P = 1–3$ bar for 7–10 days. Samples frequently fractured in the course of the experiment; when so, fluid inclusions were conserved not only in etching pits (surface inclusions) but also in fractures (fracture inclusions).

The fluid-inclusion transformation experiments simulated the isobaric cooling and isothermal compression conditions, i.e., the conditions in which the fluid in inclusions had a lower density than the external fluid in the ampoule. Effective pressure was varied from 500 to 2500 bar. In modeling isothermal compression, effective pressure was set equal to the difference between the pressure applied during the inclusion synthesis and the set (external) pressure in the model experiment. When modeling isobaric cooling, the difference between the external pressure and the pressure in the inclusion, which corresponded to the position of the isochore at a given experimental temperature, was considered.

The run parameters were the following: T = 400–700°C and P = 1–3 kbar, or T = 400–700°C and P = 3–5 kbar; the run duration was 7–10 days. Oxalic acid without water added was used as the fluid source. A set of runs was carried out using a *labeled* fluid, whose composition differed from the starting composition of the fluid inclusions. Density and composition gradients between the fluid inclusions and the external fluid in the ampoule were set in this way. The source of the external fluid in this set of runs was a salt solution (containing 25 wt % NaCl) and silver nitrate mixed with water.

Before and after the runs, inclusions were examined with a microscope and carefully documented. With rare exceptions (run 34-43), the same inclusions were studied in the starting quartz and in the run products. The carbon dioxide homogenization temperature Th_{CO_2} and melting temperature Tm_{CO_2} were measured using a Linkam THMSG 600 heating/cooling stage, which

allowed the automated (programmed) cooling/heating of the sample at rates from 0.1 to 90°C /min in the temperature interval of –195 to +600°C. The standard instrumental error was ±0.1°C. The stage was calibrated against the triple point (–56.6°C) of a CO_2 standard (Camperio, Alps) and the melting temperature of pure H_2O from synthetic fluid inclusions. The products of some experiments were quantitatively analyzed using Raman spectroscopy on a single-channel laser spectrometer at the Institute of Mineralogy and Petrography, Russian Academy of Sciences, Novosibirsk. These data were used to derive an empirical equation for the CO_2 melting temperature as a function of CH_4 concentration for methane-containing inclusions: $X_{CH_4} = -1.1576 Tm_{CO_2} - 65.565$; the mean square deviation was $R^2 = 0.9611$. This equation was used to estimate the methane concentration in inclusions. The methane concentration in the products ranged from 0.2 to 8.6 mol % (Table 1). To determine the bulk density of fluid inclusions, the volume ratios of phases for 20°C were calculated as the surface area ratio in flat inclusions and as the length ratio in cylindrical inclusions. For inclusions in which the fluid composition was known from the Raman data, pressures were calculated using the FLUIDS program package [17, 18]. The density, molar volume, and molar ratios were determined using software Program 1: BULK, version 01/02 and the equations of state borrowed from [19, 20]. The isochores were calculated using software Program 2: ISOC, version 01/02 and the equation of state from [19].

SYNTHESIS OF FLUID INCLUSIONS

Surface and fracture H_2O–CO_2–CH_4 inclusions (inclusions **A**), which are shown in Figs. 1a–1c, were synthesized at 700°C and 3 kbar using oxalic acid as the fluid source. The surface inclusions had sizes of 10–20 μm; they were isometric and flat, approaching a negative crystal to various extents. The fracture inclusions as a rule had higher volumes and were extended. The volume ratio between the fluid phases in the inclusions, $(CO_2 + CH_4)/H_2O$, averaged 0.9/0.1. At room temperature, there were two phases in the inclusions: H_2O and liquid CO_2. The homogenization temperatures of CO_2 inclusions to liquid ranged from 1.0 to 17.9°C; the melting temperatures ranged from –56.8 to –64.1° (Table 1). Methane in the inclusions was from 0.15 to 8.6 mol %. The calculated overall densities were 0.50–0.86 g/cm^3.

Inclusions **B** were synthesized using oxalic acid as the fluid source at 700°C and 1 kbar in surface pits (Fig. 1d). These were large (up to 30 μm), extended, and bulky inclusions; at room temperature, they contained two phases ($H_2O + CO_2$ liq). The CO_2 homogenization to gas temperatures ranged from 20.4 to 21.4°C; the melting temperatures were at –58.4 to –59.0°C. The $(CO_2 + CH_4)/H_2O$ volume ratios averaged 0.85/0.15. The inclusion densities were 0.34–0.38 g/cm^3.

H_2O–CO_2 surface inclusions (**C**) were synthesized from silver oxalate mixed with water at 700°C and 3 kbar (Figs. 1e–1g). The sizes and shapes of these inclusions were analogous to those of varieties **B**. At room temperatures, inclusions **C** were three phases ($H_2O + CO_2$ liq + CO_2 gas) with Th_{CO_2} = 29.4–29.8°C (to liquid) and Tm_{CO_2} at –58.8 to –59.6°C. The $(CO_2 + CH_4)/H_2O$ volume ratios averaged 0.5/0.5. The inclusion densities were 0.61–0.67 g/cm^3.

Thus, three types of inclusions were synthesized (**A**, **B,** and **C**) at different *P*–*T* parameters and/or using different fluid sources.

RESULTS OF FLUID TRANSFORMATION EXPERIMENTS

To simulate *isobaric cooling* (run 34–42), we used samples with inclusions **A** synthesized at 700°C and 3 kbar. The effective pressure was about 1 kbar. The external fluid was oxalic acid (i.e., the external fluid did not differ in its composition from the fluid entrapped in inclusions). After 7-day exposure at 400°C and 3 kbar, the transformation of vacuole walls was observed in many inclusions: faces, acute angles, serrated boundaries, and small springs appeared containing mainly an aqueous phase (Fig. 2). Such an evolution is intrinsic to fluid inclusions that experienced isobaric cooling [7, 8]. The CO_2 melting temperatures in most inclusions slightly increased after the run (Table 2), which may be a sign of the increase in the CO_2/CH_4 primary ratio. No noticeable change in Th_{CO_2} was observed; the increase in Tm_{CO_2} was observed both in cases where the inclusion shape changed and where it did not change. The reasons for this are not quite clear, although we may assume that the compositional evolution of the primary fluid is due to the leakage of hydrogen as a result of diffusion through the inclusion walls.

The most prominent alterations of the composition and density (with the shape and volume conserved) occurred in the two inclusions shown in Fig. 3. Before the run, homogenization to liquid occurred at 13.6°C in one inclusion and at 10.0°C in the other; the carbon dioxide melting occurred at –60.1 and –57.9°C, respectively (the corresponding methane concentrations were 4.0 and 1.4 mol %, respectively). The $(CO_2 + CH_4)/H_2O$ phase volume ratios calculated as the surface area ratios were 89/11 in the first inclusion and 95/5 in the second inclusion. Thus, the bulk density of the inclusions was 0.81 and 0.86 g/cm^3, respectively (Table 1). After the run, Th_{CO_2} decreased appreciably to become –1.5 and –3.5°C, respectively. The concentration of the aqueous phase increased: it was 26 vol % in the first inclusion and 24 vol % in the second. The bulk inclu-

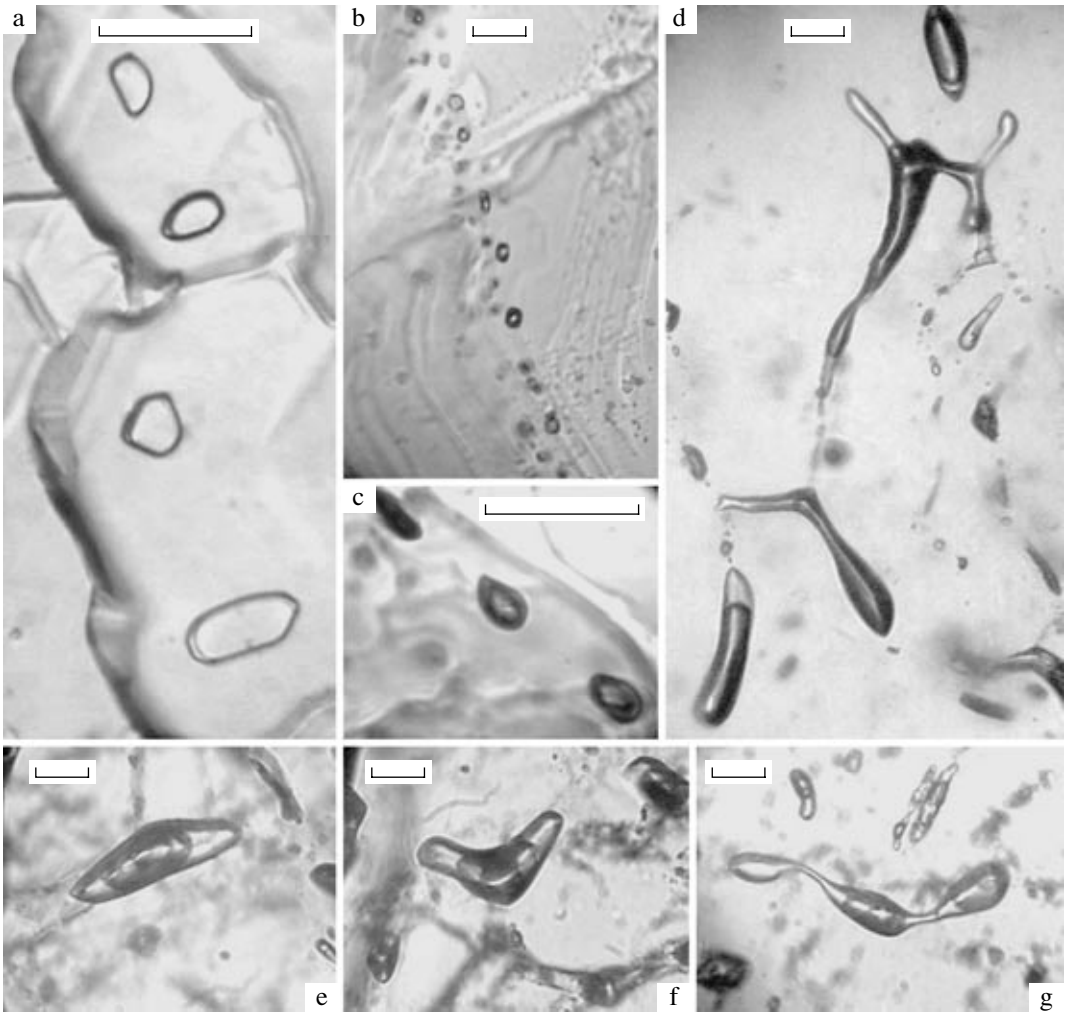

Fig. 1. Microphotographs of synthetic inclusions. Various types of inclusions: (a–c) inclusions **A**, (d) inclusion **B**, and (e–g) inclusions **C**. Scale bar: 20 μm.

sion density after the run was 0.96 and 0.93 g/cm^3, respectively (Table 1). The absence of any alterations in the volume or shape of the inclusions may indicate that the gain in the density of these inclusions was not a result of the reduction of the total volume of the vacuoles; rather, it was due to the penetration of the denser external fluid. The CO_2 melting temperatures in these inclusions changed after the run from –60.1 to –56.9°C and from –57.9 to –60.4°C, respectively. These changes, which were also observed in other cases, may arise from uncontrolled methane migration. However, this point needs special investigation.

Samples bearing inclusions **A** were also used in an experiment that simulated *isothermal compression* at 700°C and 5 kbar (run 34-43). The effective pressure was 2 kbar. As a result of this experiment, finer and denser varieties with lower CO_2 homogenization and melting temperatures were formed from inclusions **A** (Table 1). Frequently, clusters of such inclusions formed arc or half-ring structures (Fig. 4). Such structures are intrinsic to inclusions that experienced isothermal compression, which was determined experimentally [7, 8]. Their appearance is related to a change in the quartz solubility and subsequent dissolution and reprecipitation of the host mineral substance. The calculated bulk densities of inclusions after the run were 0.84–0.90 g/cm^3 against 0.84–0.85 g/cm^3 before the run (Table 1). Relatively large nascent inclusions, which were formed from large channels, had the lowest Th_{CO_2} and Tm_{CO_2}.

The set of *labeled* fluid experiments was performed on samples that contained inclusions **A**, **B**, or **C**. In the experiment with inclusions **A**, a salt solution (25 wt % NaCl) was used as the external fluid. The effective pressure was 1 kbar. As a result of isobaric cooling at 400°C and 3 kbar (run 34-48), the starting inclusions underwent several alterations: the wall shape changed; in some cases, the aqueous–salt fluid substituted for the H_2O–CO_2 fluid; several inclusions became appreciably denser; and the CO_2 melting temperatures changed

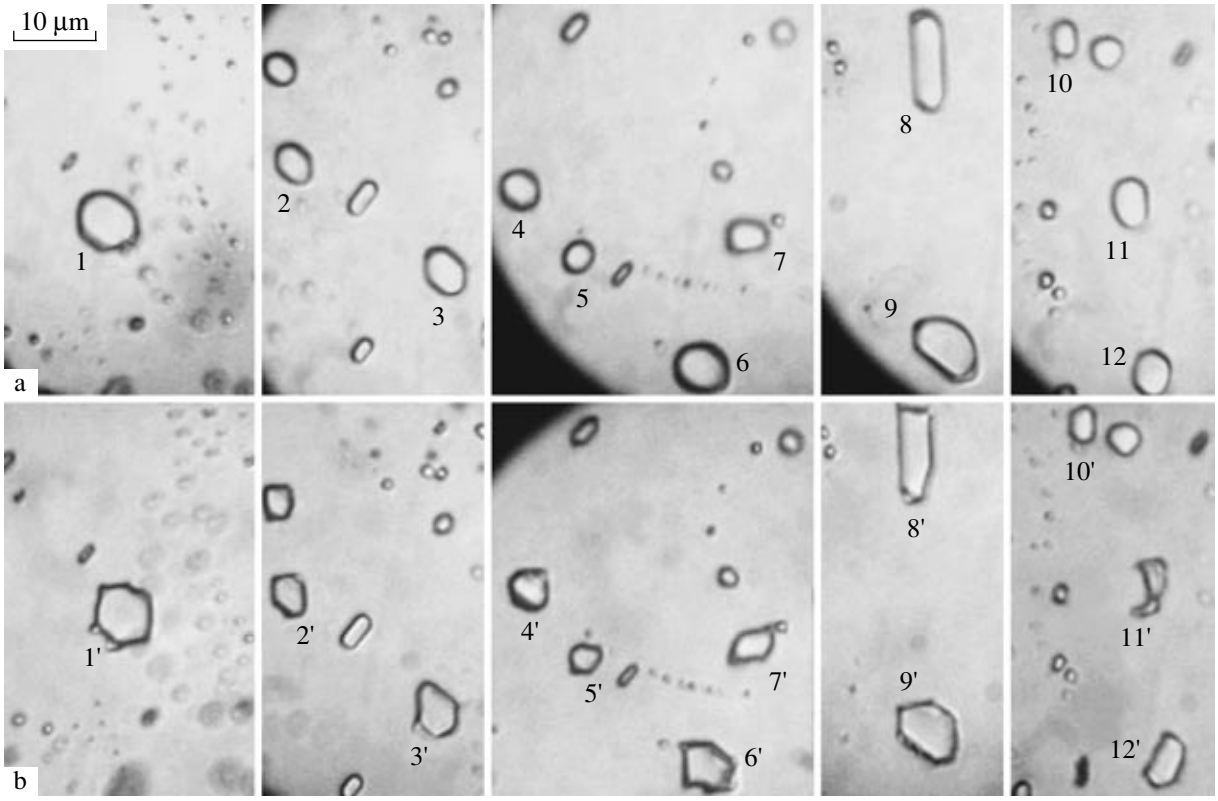

Fig. 2. Evolution of the inclusion shape in run 34-42: (a) inclusions before the run and (b) the same inclusions after the run.

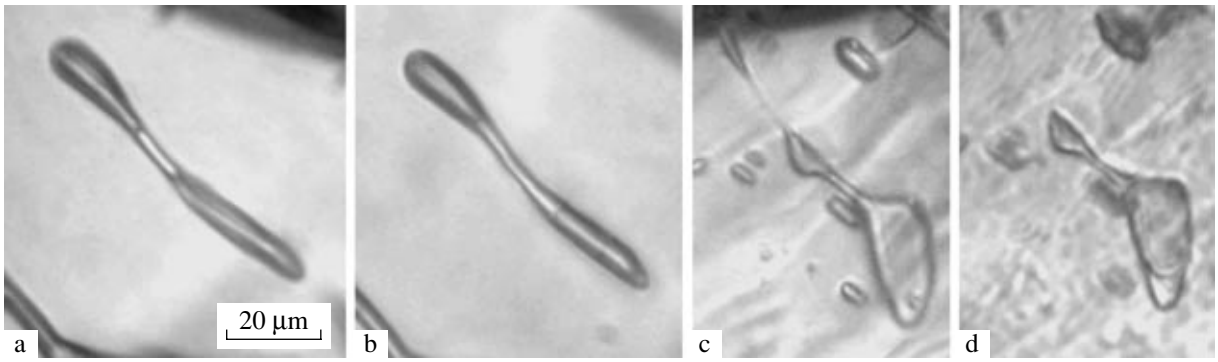

Fig. 3. Microphotographs of inclusions (run 34-42) whose composition and density experienced the greatest alteration: (a, c) inclusions before the run and (b, d) the same inclusions after the run. Scale bar: 20 μm.

without noticeable change in the homogenization temperature.

Figure 5 displays one inclusion before and after the run in which fluid substitution occurred. In the starting H_2O–CO_2 fluid, CO_2 homogenization to liquid occurred at 18.0°C. After the run, there was no carbon dioxide phase in the inclusion, and the final melting of the aqueous fluid occurred at –5.6°C, which corresponds to 8.7 wt % NaCl. Neither the volume nor the wall shape of the vacuole changed.

The density of some inclusions increased substantially after the run. In one group of inclusions, Th_{CO_2} before the run ranged from 6.9 to 12.2°C and Tm_{CO_2} from –61.2 to –62.4°C (ρ = 0.80–0.82 g/cm^3) (Table 1). After the run, Th_{CO_2} decreased to 3.4–10.5°C and Tm_{CO_2} increased to (–59.5)–(–60.9)°C; the density increased to 0.84–0.86 g/cm^3. Unfortunately, in view of the small sizes of these inclusions, we failed to measure the melting temperature of the aqueous phase; therefore, we were unable to detect the penetration of the

Table 1. Fluid inclusion data

Run no.	*PT* parameters, °C–kbar–days		Inclusion type	Before run				After run			
	synthesis	modeling		Th_{CO_2}	Tm_{CO_2}	X_{CH_4}, mol %	inclusion density, g/cm^3	Th_{CO_2},°C	Tm_{CO_2},°C	X_{CH_4}, mol %	inclusion density, g/cm^3
34-42	700-3-7	400-3-7	A	13.6	–60.1	4.0	0.81	–3.5	–56.9	0.3	0.96
				10.0	–57.9	1.4	0.86	–1.5	–60.4	4.3	0.93
				4.9–17.3	–57.1– –64.1	0.5–8.6	0.79–0.83	4.9–15.5	–58.8– –61.2	2.3–5.2	0.82–0.85
34-43	700-3-7	700-5-7	A	2.9–15.4	–58.1– –61.6	1.7–5.7	0.84–0.85	–8.8–10.8	–57.4– –62.1	0.9–6.3	0.84–0.90
34-48	700-3-7	400-3-10	A	18.0	–57.4	0.9	_	aq	–5.6	_	_
				6.9–12.2	–61.1	5.1	0.80–0.82	3.4–10.5	–59.5	3.3	0.84–0.86
				1.0–17.9	–56.8– –63.3	0.2–7.7	0.51–0.84	1.1–17.8	–57.2– –62.0	0.6–6.2	0.74–0.85
52-53	700-3-10	400-3-10	C	29.4–29.8	–58.8– –59.6	2.5–3.4	0.72	–31.2– –29.5	–60.4– –64.1	4.3–8.6	_
41-44	700-1-6	400-1-7	B	20.4–21.4(g)	–58.4– –59.0	2.0–2.7	0.34–0.38	16.6(nc)–19.5(g)	–58.4– –59.0	2.0–2.7	0.31
								17.3–18.3(cr)	–60.1	4.0	0.48–0.49
44-46	400-1-7	400-3-9	B	16.6(nc)–19.5(g)	–58.4– –59.0	2.0–2.7	0.31	17.6–20.5(g) + aq	–60.3– –60.4 + aq (–4.8)	4.2–4.3	0.33
			B1	17.3–18.3(cr)	–60.1	3.97	0.48–0.49	17.8–-18.0(cr)	–60.3	4.2	0.48–0.49
					_	_		aq	–9.8– –16.5	_	_

Note: Homogenization types: (g) into gas; (cr) critical; (nc) near-critical; aq—salt-aqueous fluid inclusions.

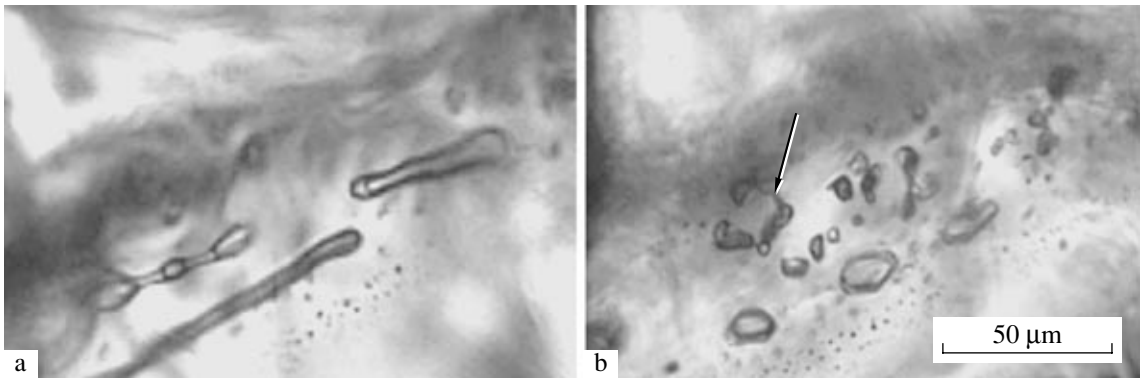

Fig. 4. Modeling of isothermal compression (run 34-43): (a) inclusions before the run and (b) the same region of the sample after the run. The arrow marks newly formed half-ring textures. Scale bar: 50 μm.

external fluid into these inclusions. Neither the size nor the shape of the inclusions changed.

As a result of run 34-48 (as after run 34-42), $T\mathrm{m}_{\mathrm{CO}_2}$ changed in many inclusions while $T\mathrm{h}_{\mathrm{CO}_2}$ did not change significantly. As a rule, this change was an increase; the CO_2 melting temperature decreased only in few inclusions. The wall shape changed, like in run 34-42, only in a few cases.

The experimental modeling of isobaric cooling at 400°C and 3 kbar using silver nitrate mixed with water as the external fluid source was performed on samples containing H_2O-CO_2 surface inclusions **C** (Table 1). The effective pressure was 1.5 kbar. The composition of the fluid in the ampoule was set by powdered silver nitrate (180 mg) and water (0.04 ml). For most inclusions, the vacuole shape changed after the run to a greater degree than in the previous runs: their walls acquired a well-defined serrated shape.

The starting inclusions were uniform in their composition and density: $T\mathrm{h}_{\mathrm{CO}_2}$ = 29.4–29.8°C, and $T\mathrm{m}_{\mathrm{CO}_2}$ ranged from –58.8 to –59.6°C. After the run, a significant scatter appeared in the homogenization temperatures (from –31.2 to 29.5°C) and melting temperatures (from –59.2 to –64.1°C) in the inclusions (Table 1).

In all cases, fluid heterogenization preceded the freezing of the aqueous phase. Figure 6 shows one inclusion before and after the run. Before the run, the inclusion contained an aqueous phase and a carbon dioxide phase. The carbon dioxide homogenization (to liquid) temperature was 29.8°C, and the carbon dioxide melting temperature was –59.1°C. The bulk fluid density was 0.72 g/cm^3. After the run, both the homogenization to liquid temperature and melting temperature of carbon dioxide depressed dramatically to –31.2 and –64.1°C, respectively. The phase ratio also changed toward the decreasing volume of the carbon dioxide component. It is significant that the composition of the aqueous phase also changed: the aqueous phase turned light brown when frozen. The volume of the inclusion did not change appreciably. These results unambiguously signify an appreciable increase in the density of the primary inclusion due to the penetration of the denser nitric–aqueous external fluid. Characteristically,

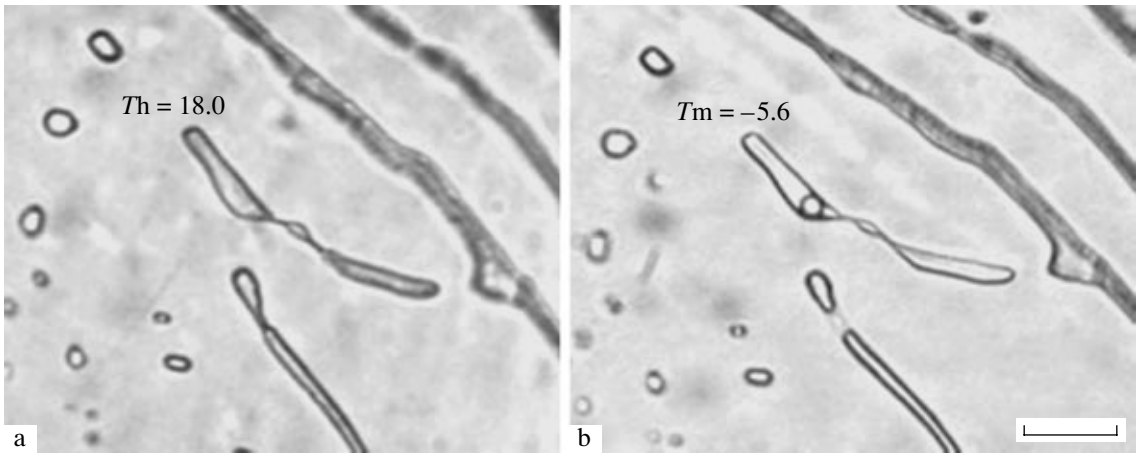

Fig. 5. Modeling of isobaric cooling by the *labeled* fluid method (run 34-48): (a) an inclusion before the run with $T\mathrm{h}_{\mathrm{CO}_2}$ = 18.0°C and (b) the same inclusion after the run with the final melting of the aqueous fluid at –5.6°C. Scale bar: 20 μm.

not only did the gas phase change its composition (evidently due to nitrogen or, possibly, nitrogen oxides), but also the aqueous phase changed its composition as a result of mixing with the silver-containing external fluid, which was proven by the color of the frozen fluid. In some other inclusions, carbon dioxide did not heterogenize tile the aqueous phase froze (which occurred at about –35°C); when frozen, the aqueous phase turned dark brown and became unclear. Unfortunately, this fact inhibited further cryometric investigations of the inclusions. On the whole, the composition of the fluid entrapped into various inclusions varied widely, as shown by the melting temperatures of the fluid and the color of the frozen fluid.

Two sets of runs were carried out with samples containing inclusions **B** and synthesized at 700°C and 1 kbar. In the first set (run 41-44), isobaric cooling at 400°C and 1 kbar was modeled in the presence of the fluid of the same composition (with oxalic acid as the external fluid source). The effective pressure was 500 bar. As a result of the run, a new generation of inclusions (**B1**) formed on the surface of the quartz rod with near-critical homogenization (a gas bubble grew in size and gradually disappeared); Th_{CO_2} = 17.3–18.3°C, Tm_{CO_2} = –60.1°C, and the $(CO_2 + CH_4)/H_2O$ volume ratio was 65/35. The densities calculated for these inclusions (0.48–0.49 g/cm^3) were slightly higher than for the initial inclusions (0.34–0.38 g/cm^3).

Most of the initial inclusions **B** (which were synthesized at 700°C and 1 kbar) did not change their shapes after the run. A small depression of the homogenization (to gas) temperature that occurred corresponded to the decrease in the density to 0.31 g/cm^3 (Table 1). This decrease under the denser external fluid settings may be due to some loss of the fluid during the putting of the run into or out of the working regime.

Table 2. Cryometric data (Tm_{CO_2} and Th_{CO_2}) for inclusions shown in Fig. 2. For all inclusions, the homogenization type was gas ⟶ liquid

Inclsion no.	Tm_{CO_2}	Th_{CO_2}	Incluion no.	Tm_{CO_2}	Th_{CO_2}
1	–62.2	7.5	1	–60.7	7.7
2	–	9.5	2'	–	8.3
3	–62.2	9.5	3'	–60.4	8.5
4	–	8.1	4'	–	8.2
5	–	8.7	5'	–	8.7
6	–62.2	7.8	6'	–60.8	7.5
7	–	8	7'	–	8.1
8	–61.2	11	8'	–59.6	10.8
9	–61.2	11.1	9'	–59.6	10.9
10	–	9.5	10'	–	9.4
11	–61.2	9.5	11'	–	8.5
12	–61.2	9.5	12'	–	9.1

In the second set of runs (run 44-46), the products obtained in the first set were used as the starting material. Isothermal compression at 400°C and 3 kbar in the presence of an external aqueous fluid (25 wt % NaCl) was modeled. The effective pressure was 2.5 kbar for the first generation and 2.3 kbar for the second one.

As a result of the run, some second-generation inclusions (formed at 400°C and 1 kbar) changed their composition to the salt–aqueous fluid with the final melting point of ice ranging from –9.8 to –16.5°C (Table 1); the corresponding NaCl concentrations ranged from 13.8 to 20.0 wt %. These inclusions did not contain carbon dioxide; i.e., the salt–aqueous fluid substituted for their

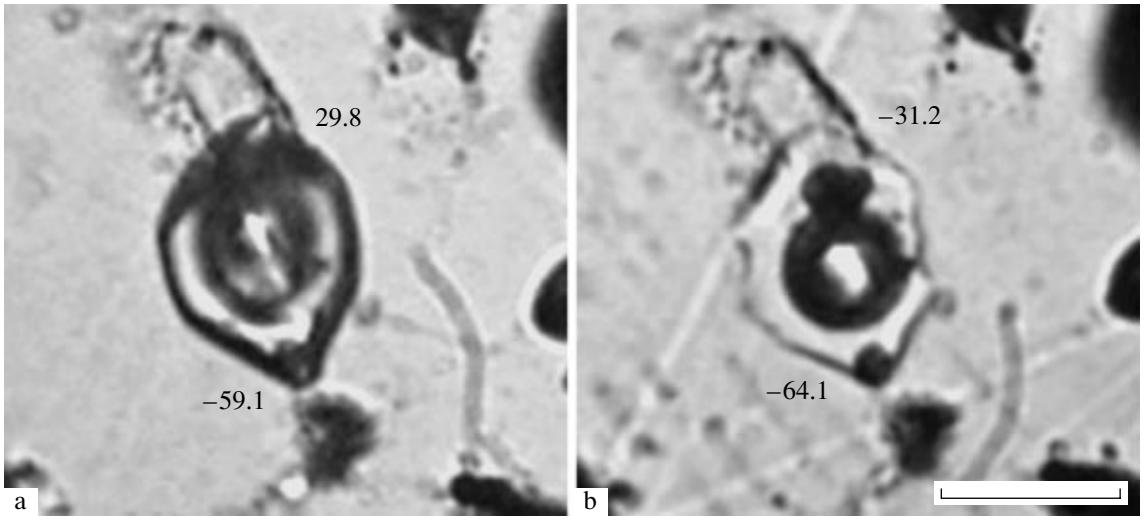

Fig. 6. Modeling of isobaric cooling by the *labeled* fluid method (run 52-53): (a) an inclusion before the run and (b) the same inclusion after the run. The figures indicate Th_{CO_2} and Tm_{CO_2}. The alteration of the volume phase ratios is well defined. Scale bar: 20 μm.

starting gaseous component. In the other varieties of this generation, there were no noticeable changes in the density, composition, or shape of inclusions (Table 1). In the vast majority of the first-generation inclusions **B**, vacuole walls changed significantly: they became serrated. However, the composition and density changed substantially only in several cases.

Figure 7 shows one such inclusion before and after the run. Before the run, the inclusion contained an H_2O–CO_2–CH_4 fluid with Th_{CO_2} = 17.4°C (to gas) and Tm_{CO_2}= –59.0°C, which corresponds to a density of 0.31 g/cm^3. After the run, the fluid composition changed to a CO_2–aqueous fluid with near-critical CO_2 homogenization with Th_{CO_2} = 17.5°C and Tm_{CO_2} = –60.4°C and with the ice melting temperature equal to –4.8°C. The exact determination of the volume phase ratio for this inclusion was impossible because its walls were heavily serrated. The overall fluid density was estimated at 0.33 g/cm^3 on the assumption that the (CO_2 + CH_4)/H_2O volume ratio was constant. In general, the fluid density increased with increasing aqueous-phase volume in the inclusion. Therefore, we may assume that the calculated density was even an underestimate: evidently, the concentration of the aqueous phase in the inclusion was higher than the initial value because of the entrance of the aqueous fluid. It is also significant that the vacuole shape altered only in inclusions **B**. Such alterations may be associated with the recrystallization of the inclusion walls: the penetration of the external fluid induced dissolution and reprecipitation of the matter at the quartz–fluid interface. The penetration of the fluid was evidently enhanced by the comparatively higher dislocation density of these inclusions after additional isobaric cooling.

DISCUSSION

The above experimental data show that isobaric cooling and isothermal compression induced changes in the shape, composition, and density of primary H_2O–CO_2–CH_4 inclusions. The extent of these changes was usually differentiated even within one sample.

Inclusion Shape

The shape of inclusion walls changed in all runs except for run 41-44; as a rule, the shape changed in the inclusions in which the fluid composition did not change appreciably. Faces, acute angles, and serrated boundaries appeared during isobaric cooling, and the aqueous phase concentrated in small springs. The intensity of the shape alteration increased with increasing aqueous-phase concentration in the inclusions. For example, in run 52-53 with 50 vol % of aqueous phase, the alteration of the inclusion shape was more prominent and was observed in more inclusions than in runs 34-42 and 34-48, in which the concentration of the aqueous phase was as low as 10%.

During isothermal compression, either arc structures were generated (in run 34-43) or inclusion walls substantially recrystallized (in run 44-46).

Our data agree with the inferences made by many researchers [21, 10, 22, 8, and others]: it was inferred in the works cited that the dissolution and reprecipitation of the host mineral substance was responsible for the alteration of the inclusion walls, and the intensity of these alterations was a direct function of the pressure and temperature difference and of the amount of water in the inclusion. Isothermal compressions at a pressure difference of 4.1 kbar did not induce any shape alteration in the CH_4 inclusions that were free of an aqueous phase or contained it in minimal amounts in the form of a thin film on the vacuole walls [15]. In aqueous or salt–aqueous inclusions, not only did inclusion walls change but also satellite inclusions were formed even when the pressure difference was as low as 1.8 kbar [10].

Inclusion Density

The density of fluid inclusions increased in all experiments (except for run 41-44); this increase varied from insignificant (0.06 g/cm^3 in run 44-46) to fairly noticeable (0.15 g/cm^3 in run 34-42). Unambiguously, the inclusion volume did not usually change when the inclusion density increased substantially, but as a rule, the water/gas ratio increased and the component composition changed; this was demonstrated by the results of the *labeled* fluid experiments (runs 44-46, 52-53).

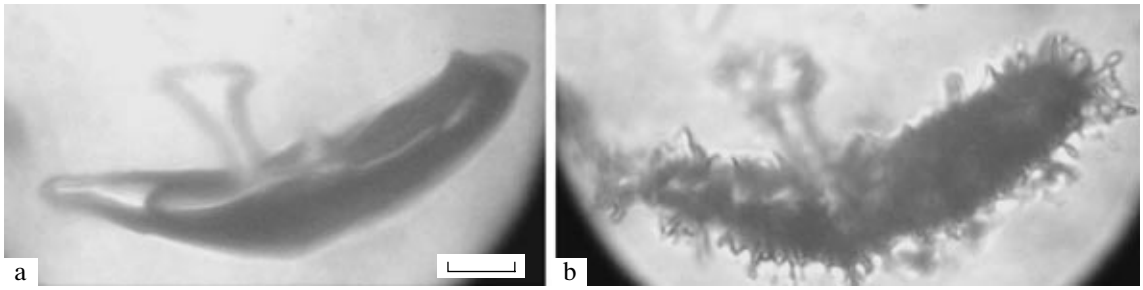

Fig. 7. Evolution of the inclusion wall shape induced by isothermal compression: (a) an inclusion before the run and (b) the same inclusion after the run. Scale bar: 10 μm.

These results signify that the penetration of the denser external fluid into less dense fluid inclusions was the main scenario of increasing inclusion density at the given *pT* conditions. We did not observe a change in the composition of the aqueous phase (i.e., the penetration of the external fluid into inclusions) only in one group of very fine inclusions (run 34-48); the density of these inclusions increased from 0.80–0.82 to 0.84–0.86 g/cm^3 as a result of the experiment.

Inclusion Composition

The inclusion composition varied differently, even within individual samples. The external fluid (in runs 34-48, 44-46, 52-53) substituted for the initial fluid in the inclusions. It was shown experimentally that any inclusion is associated with at least several dislocations or even microfractures and the dislocation density around the inclusion increases under changing external *P–T* parameters [13, 9, 14]. It was also proven in [13, 9, 14] that water leakage from the inclusions is mainly due to fluid migration along such dislocations and microfractures rather than to diffusion through the inclusion walls. However, the fluid can also move in the opposite direction along dislocations. In the products of several experiments, inclusions contained increased NaCl concentrations, which resulted from fluid exchange with the environment through dislocations [23].

Thus, we may assume that the most likely scenario of the transformation of the composition and density of inclusions in our experiments was the migration of the fluid from the environment along microfractures and dislocations. Several experiments showed changed methane concentrations in fluid inclusions; these changes were measured as a change in the carbon dioxide melting temperature (in all runs but run 41-44), which was not accompanied by any noticeable change in the homogenization temperature. This process is yet poorly understood, but we tend to think that hydrogen diffusion induced the aforementioned changes in the methane concentration in inclusions.

Our results show that the degree of transformation of fluid inclusions (including the density change) was affected by the permeability of the inclusions, i.e., their accessibility to the external fluid. The accessibility, in turn, depended on the degree of deformation of the host mineral, its perfection, and other factors. Certainly, natural conditions differ significantly from experimental ones in the exposure period; a far greater share of primary inclusions is expected to experience an increase in density during retrograde metamorphism in nature. We think, however, that there is a rather high probability of the conservation of primary, untransformed inclusions in such rocks (in parts of minerals least accessible to the external fluid), which is frequently manifested in the investigations of natural complexes, including metamorphic ones. This allows us to meet with optimism investigations of fluid inclusions intending to reconstruct the physicochemical conditions of not only retrograde mineral formation, but of primary mineral formation also.

CONCLUSIONS

In our experiments, we did not find adequate evidence that the inclusion density increased as a result of decreasing inclusion volume. In general, the simulation experiments by other researchers also failed to prove this unambiguously. From our data, we may infer that the penetration of a denser external fluid into less dense fluid inclusions is the main scenario of the compositional alteration and increase in the density of H_2O–CO_2–CH_4 inclusions during isobaric cooling and isothermal compression (within the range of the *P–T* parameters studied). In principle, this scenario is an absolute analog of a decrease in the density of fluid inclusions during their retrograde evolution. The final result (either an external fluid penetrated into inclusions, or it leaked into the ambience) is determined only by the relative position of the isochores of the fluid in inclusions and the *P–T* trends of tectonothermal events in the region [24]. The absence of the signs of inclusion density increasing as a result of decreasing volume does not rule out, however, the possibility for this scenario to come into play. This may signify that some conditions other than the simulated ones may exist under which density increasing results from decreasing volume; for example, stresses may induce plastic deformations in minerals, in particular, on the crystal-lattice scale. This possibility has not been experimentally checked. However, the reconstruction of the physicochemical conditions of geological processes, in particular, metamorphism, may give essential information about the evolution scenarios of fluid inclusions and, finally, about the evolution paths and fluid regime of metamorphism itself. For example, superdense inclusions with the higher *P–T* parameters of entrapment compared to the *P–T* conditions of peak metamorphism can form as a result of the entrapment of a new, denser inclusion generation during isobaric cooling and not due to an increase in the density of the previously entrapped varieties. A similar case was in fact modeled in the set of runs carried out on samples containing inclusions **B** (Table 1). We also discovered it when investigated metamorphic conditions in rocks from the Trivandrum granulite block, Southern India [6]. Here, a genetically autonomous group of relatively late (undoubtedly, secondary) inclusions, which were far denser than primary peak varieties, was discovered. These inclusions were formed directly at low subisobaric cooling temperatures due to the conditions of brittle deformations and the development of intense fracturing in minerals.

In summary, our experimental modeling showed that during retrograde metamorphic evolution, the density of fluid inclusions not only can decrease, which is the most common process in natural setting, but they can also increase. Superdense inclusions may form as a

result of the following two processes: either their density increases because of the penetration of a denser external fluid into less dense fluid inclusions or new generations of dense inclusions are entrapped by minerals that underwent brittle deformation with fracturing. The formation of superdense inclusions due to the deformation (a decrease in the size) of vacuoles also cannot be ruled out. However, the scenarios of this process need experimental verification.

ACKNOWLEDGMENTS

The authors thank A.A. Tomilenko (Institute of Mineralogy and Petrography, Siberian Division, Russian Academy of Sciences, Novosibirsk) for assistance in qualitative and quantitative Raman analysis, L.Yu. Zharikova for her activity in the first stages of the work, and Z.A. Kotel'nikova and V.B. Naumov for constructive criticism, which was taken into account in the final version of the manuscript.

This work was supported by the Russian Foundation for Basic Research (project nos. 01-05-65013, 01-05-65018, 04-05-65109, 04-05-64585).

REFERENCES

1. L. S. Hollister, "Enrichment of CO_2 in Fluid Inclusions in Quartz by Removal of H_2O during Crystal-Plastic Deformation," J. Struct. Geol. **12**, 895–901 (1990).
2. H. E. C. Swanenberg, "Fluid Inclusions in High-Grade Metamorphic Rocks from S.W. Norway," Geol. Ultraiectina **25**, 147 (1980).
3. V. I. Fonarev, J. L. R. Touret, and Z. A. Kotelnikova, "Fluid Inclusions in Rocks from the Central Kola Granulite Area (Baltic Shield)," Eur. J. Mineral. **10**, 1181–1200 (1998).
4. V. I. Fonarev and R. Kreulen, "Polymetamorphism in the Lapland Granulite Belt: Evidence from Fluid Inclusions," Petrology **3**, 340–356 (1995).
5. A. M. Kerkhof and S. Olsen, "A Natural Example of Superdense Inclusions: Microthermometry and Raman Analysis," Geochim. Cosmochim. Acta **54**, 895–901 (1990).
6. V. I. Fonarev, M. Santosh, O. V. Vasiukova, and M. B. Filimonov, "Fluid Evolution and Exhumation Path of the Trivandrum Granulite Block, Southern India," Contrib. Mineral. Petrol. **145**, 339–354 (2003).
7. S. M. Sterner and R. J. Bodnar, "Synthetic Fluid Inclusions. VII. Re-Equilibration of Fluid Inclusions in Quartz during Laboratory-Simulated Metamorphic Burial and Uplift," J. Metamorph. Geol. **7**, 243–260 (1989).
8. M. O. Vityk and R. J. Bodnar, "Textural Evolution of Synthetic Fluid Inclusions in Quartz during Reequilibration, with Application to Tectonic Reconstruction," Contrib. Mineral. Petrol. **121**, 309–323 (1995).
9. M. O. Vityk and R. J. Bodnar, "Synthetic Fluid Inclusions. XV. TEM Investigation of Plastic Flow Associated with Reequilibration of Fluid Inclusion in Natural Quartz," Contrib. Mineral. Petrol. **139**, 285–297 (2000).
10. M. O. Vityk, R. J. Bodnar, and C. S. Schmidt, "Fluid Inclusions as Tectonothermobarometers: Relation between Pressure–Temperature History and Reequilibration Morphology during Crustal Thickening," Geology **22**, 731–734 (1994).
11. R. J. Bakker and J. B. H. Jansen, "Preferential Water Leakage from Fluid Inclusions by Means of Mobile Dislocations," Nature **345**, 58–60 (1990).
12. R. J. Bakker and J. B. H. Jansen, "Experimental Post-Entrapment Water Loss from Synthetic CO_2–H_2O Inclusions in Natural Quartz," Geochim. Cosmochim. Acta **55**, 2215–2230 (1991).
13. R. J. Bakker and J. B. H. Jansen, "A Mechanism for Preferential H_2O Leakage from Fluid Inclusions in Quartz, Based on TEM Observations," Contrib. Mineral. Petrol. **116**, 7–20 (1994).
14. Z. A. Kotel'nikova and V. E. Sonyushkin, "Dislocation Structure of Quartz and Problems of Closeness of Fluid Inclusion Cavities," Zap. Vses. Mineral. O–va, No. 3, 9–19 (1994).
15. V. A. Kalyuzhnyi, "The Peculiarities of the Evolution of Hydrothermal Fluids $H_2O + CH_4 + C_nH_m$ as a Medium of Rock-Crystal ('Marmarosh Diamonds') Crystallization from the Ukrainian Carpathians," Arch. Mineralogic. **49**, 109–110 (1993).
16. W. C. Luth and O. F. Tuttle, "Externally Heated Pressure Vessels for Use to 10,000 Bars and 750°C," Am. Mineral. **48**, 1401–1403 (1963).
17. R. J. Bakker, "FLUIDS: New Software Package to Handle Microthermometric Data and to Calculate Isochors," in *Proceedings of 16th ECROFI European Current Research on Fluid Inclusions, Porto, Portugal, 2001*, Ed. by F. Noronha, A. Doria, and A. Guedes, (Mem. Faculd. Ciencias Porto, 2001), Vol. 7, pp. 23–25.
18. R. J. Bakker, "Package FLUIDS 1. Computer Programs for Analysis of Fluid Inclusion Data and for Modelling Bulk Fluid Properties," Chem. Geol. **194**, 3–23 (2003).
19. Z. Duan, N. Moller, and J. H. Weare, "A General Equation of State for Supercritical Fluid Mixtures and Molecular Dynamics Simulation of Mixture *PVTX* Properties," Geochim. Cosmochim. Acta **60**, 1209–1216 (1996).
20. R. Thiéry, A. M. Kerkhof, and J. Dubessy, "*VX* Properties of CH_4–CO_2 and CO_2–N_2 Fluid Inclusions: Modeling for $T < 31°C$ and $P < 400$ bars," Eur. J. Mineral. **6**, 753–771 (1994).
21. R. J. Bodnar, "Reequilibration of Fluid Inclusions," in *Fluid Inclusions: Analysis and Interpretation*, Ed. by I. Samson, A. Anderson and D. Marshall, Mineral. Assoc. Can., Short Course **32**, 213–230 (2003).
22. M. O. Vityk, R. J. Bodnar, and I. Dudok, "Natural and Synthetic Reequilibration Textures of Fluid Inclusions in Quartz (Marmarosh Diamonds): Evidence for Refilling under Conditions of Compressive Loading," Eur. J. Mineral. **7**, 1071–1087 (1995).
23. Z. A. Kotel'nikova, "Properties of Fluid Inclusions during a Change in Environmental Physicochemical Parameters: An Experimental Study," Geokhimiya, No. 4, 476–485 (1994).
24. J. L. R. Touret, "Fluids in Metamorphic Rocks," Lithos **55**, 1–25 (2001).